Adaptive Memory-Polarization for Improved Performance of Mho Relay in Presence of Grid-Following PV

Meenu Jayamohan, Sarasij Das, Jose de Jesus Chavez, Marjan Popov

***Abstract*—This paper addresses the challenges posed by high Grid-Following (GFOL) Photovoltaic (PV) penetration on the dynamic performance of memory-polarized mho relays, crucial for close-in fault protection in power systems. Traditional memory-polarized mho relays, designed for synchronous generator-dominated systems, utilize a scalar weight to dynamically expand their mho characteristics based on memory voltage, enhancing resistive reach. However, the unique transient behavior of Inverter-Based Resources (IBRs) like GFOL PV during faults can disrupt this mechanism, compromising relay reliability. To overcome this limitation, this research introduces a novel algorithm that employs a complex weight parameter in the memory polarization process, replacing the conventional scalar approach. This complex weight allows for more precise and adaptable control of the mho characteristic's dynamic expansion, enabling the relay to better respond to the complex voltage and current transients introduced by GFOL PV. The study investigates the dynamic expansion of the mho element's maximum diameter (d_{max}) and memory vector angle (θ_m) under various fault scenarios (three-phase, single-line-to-ground, and line-to-line) to evaluate the algorithm's effectiveness. The proposed complex weight algorithm is validated across diverse fault types, varying complex weight factors, and different fault resistances, considering GFOL PV generators with reactive power priority and IEEE Standard 2800-2022 compliant Low/High Voltage Ride-Through capabilities. The results demonstrate significantly enhanced reliability and stability of memory-polarized mho relays in systems with high GFOL PV penetration, showcasing the superior performance of the complex weight approach.**

***Keywords*—Grid following PV, inverter-based resources, memory-polarization, mho relay**

I. Introduction

Integrating power electronic converters into bulk power systems has significantly transformed operational characteristics. The growing penetration of Inverter-Based Resources (IBRs), such as wind and solar power plants, introduces notable changes to the dynamic behavior of the grid. Historically, synchronous generators have served as the cornerstone of power systems, providing inertia and playing a critical role in ensuring system stability. In contrast, IBRs are connected to the grid via power electronic converters and exhibit different characteristics. Typically, they function in Grid Following (GFOL) mode, synchronizing their output to the grid's voltage and frequency [1]. The increasing presence of IBR poses several challenges to power system protection. A primary concern is reducing fault current levels, as power electronic converters inherently limit fault current magnitudes [2]. This reduction can compromise the effectiveness of traditional protection schemes designed for Synchronous Generator (SG) only systems with higher fault currents [3]. Additionally, the lower inertia associated with IBRs can also impact system stability during fault conditions. These evolving system dynamics underscore the need for a comprehensive review and potential redesign of existing protection schemes. Advanced protection algorithms and technologies are essential to ensure the reliable and secure operation of power systems with high levels of IBR penetration. References [3]-[6] document the challenges posed by IBRs to distance protection elements, including maloperation stemming from reduced fault current, low fault voltage affecting polarizing voltages and the change in source voltage phase angle with respect to prefault voltage.

Memory polarization techniques are extensively utilized in mho elements for transmission line protection to detect close-in faults [7]. These elements operate on the principle that, during a fault, the voltage magnitude changes rapidly while the phase angle and frequency remain largely stable. Another critical assumption is the steady and predictable nature of the source impedance magnitude behind the relay, which allows for an accurate estimation of the increased resistive reach [7]. While this assumption is valid for systems dominated by synchronous generators (SGs), it may not hold for systems incorporating Inverter-Based Resources (IBRs), as the phase angle can deviate significantly from its pre-fault value [6].

Studies such as [8] and [9] examine the impact of IBRs on mho characteristics-based relay elements. A novel polarizing logic for distance protection element has been presented in [10] for low inertia systems. An enhanced distance relay algorithm for converter-dominated network has been discussed in [11]. Reference [12] proposes a novel offset-mho characteristic for memory-polarized relays. Additionally, the effects of PV generation with $V_{dc}Q$ control and PQ control on Positive Sequence Memory Polarized (PSMP) mho relays are analyzed in [13] and [14], respectively. A novel method to find the offset mho characteristics of

M. Jayamohan and S. Das are with Department of Electrical Engineering, Indian Institute of Science, Bangalore, India (e-mail: meenuj@iisc.ac.in, e-mail of corresponding author: sarasij@iisc.ac.in).
J. J. Chavez is with School of Engineering & Sciences, Tecnologico de Monterrey, Guadalajara, Mexico (e-mail: j.j.chavezmuro@tec.mx).
M. Popov is with Faculty of EEMCS, Delft University of Technology, Delft, The Netherlands (e-mail: M.Popov@tudelft.nl).

Paper submitted to the International Conference on Power Systems Transients (IPST2025) in Guadalajara, Mexico, June 8-12, 2025.

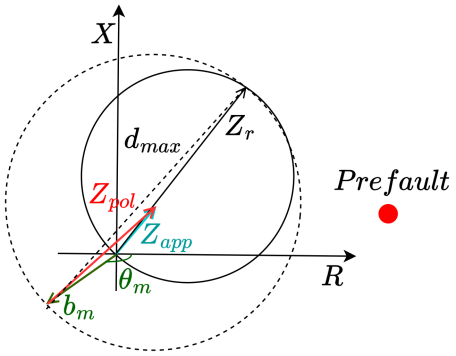

Fig. 1. Dynamic mho expansion for SG-only system

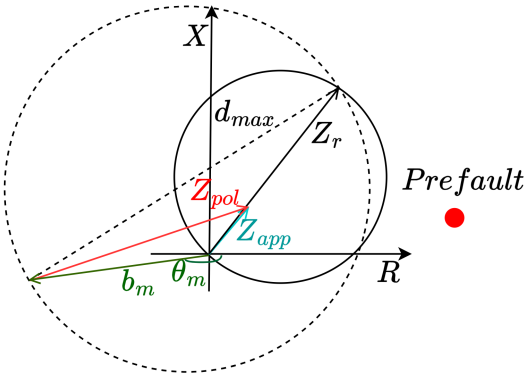

Fig. 2. Dynamic mho expansion for GFOL PV integrated system

memory and cross-polarized distance elements is presented in [15]. However, these studies [8]-[15] do not account for the performance requirements outlined in IEEE Standard 2800-2022 [16], which are critical for IBR-dominated systems. The benefits of implementing the IEEE Standard 2800-2022 to enhance various transmission line distance protection functions, including mho elements, are explored in detail in [17]. Reference [18] considers the IEEE Standard 2800-2022 and analyses the dynamic mho expansion during IBR integration for varying phase-locked loop parameters. A notable observation in IBR-integrated systems is a reduction in the resistive reach of dynamically expanded memory-polarized mho relay elements, as documented in [13] and [18]. This phenomenon has been identified, however, it has not been extensively investigated in the existing literature. To address this limitation, this paper introduces an adaptive memory polarization algorithm specifically designed to mitigate the previously mentioned challenges associated with memory-polarized mho relays operating within IBR-integrated power systems.

The major contributions of this work are presented below.

- The dynamic mho expansion of memory-polarized mho relay has been studied for three-phase-to-ground, single-line-to-ground, and line-to-line fault scenarios. Two different relay locations are considered, where the fault current seen by the relays, $R1$ and $R2$, is fully supplied by the PV generators.
- The diameter of the dynamic memory-polarized mho element's maximum expansion, d_{max}, and the angle of the memory vector, θ_m, have been examined.
- A novel algorithm that enhances the reliability of memory-polarized mho relays in the presence of GFOL PV generation has been proposed.
- The proposed adaptive algorithm has been verified for close-in faults in a GFOL PV integrated system by varying fault types, weight factors of memory polarization, and fault resistances.

II. Memory-Polarized Mho Relay

In mho relay elements, Z_{pol} and Z_{op} represent the polarizing and operating impedances, respectively. The relay's reach setting, Z_r, corresponds to the transmission line segment impedance that is being protected. The apparent impedance, Z_{app}, as observed by the relay, is determined using system voltages and currents. The mho element calculates its operating impedance as Z_{op}= Z_r-Z_{pol}. The characteristics of self-polarized mho relays are discussed in [13], [14]. However, their limitations under close-in fault conditions necessitated the development of memory polarization techniques.

In a self-polarized mho relay, the polarizing quantity in the voltage plane is the faulted phase voltage. During close-in faults, this voltage may approach or equal zero, making it insufficient to polarize the relay element. To address this, memory polarization is employed to enhance reliability. Memory polarization uses positive-sequence memory voltage or pre-fault voltage as the polarizing quantity. Positive Sequence Memory Polarized (PSMP) mho relays, widely utilized in transmission line protection, use the positive sequence pre-fault voltage instead of the faulted voltage as the polarizing quantity. Since the pre-fault voltage remains close to its nominal value even during faults, it provides adequate polarization for the relay, unlike the self-polarized variant. The term "memory voltage" refers to this pre-fault voltage generated by a memory filter [19], [20]. The memory voltage experiences a gradual and progressive shift towards the actual fault voltage over time. For a memory-polarized mho relay, Z_{pol} is computed using the fault current (I_{rf}) and the positive sequence memory voltage ($V^+_{f,m}$) or pre-fault voltage. In the i^{th} iteration of the protection pass, the memory voltage is defined as:

$$V^+_{f,m}(i) = \omega_m.V^+_f(i) + (1-\omega_m).V^+_{f,m}(i-j) \qquad (1)$$

where $V^+_{f,m}$ is the positive sequence memory voltage phasor, V^+_f denotes the positive sequence faulted phase voltage phasor, and ω_m is the weight factor, ranging between 0 and 1. The voltage from the $i-j$ protection pass serves as the memory voltage for the i^{th} protection pass. The polarizing memory voltage also serves to dynamically expand the mho characteristic. The dynamic expansion of the PSMP mho characteristic for a three-phase-to-ground fault in a system with only SGs is illustrated in Fig. 1. The vector b_m represents the memory vector and θ_m is the angle of the memory vector relative to the positive resistance axis (R-axis). The

apparent impedance (Z_{app}) and polarizing impedance (Z_{pol}) are computed as follows:

$$Z_{app}(i) = \frac{V_{rf}(i)}{I_{rf}(i)}; \qquad Z_{pol}(i) = \frac{V^{+}_{f,m}(i)}{I_{rf}(i)} \tag{2}$$

The fault current, fault voltage, and the polarizing voltage used for different types of faults considered in this paper are detailed in Table I where a=1$\angle$120° and zero sequence compensation factor K_0=0.5, where K_0=($Z_0 - Z_1$)/Z_1 [14]. The memory vector, b_m, and the diameter of the dynamic mho circle, d_m are calculated as

$$b_m(i) = Z_{app}(i) - Z_{pol}(i); \quad d_m(i) = |Z_r(i) - b_m(i)| \tag{3}$$

The maximum value of the dynamic mho expansion, denoted as d_{max}, represents the upper limit of $d_m(i)$. The corresponding angle of b_m for the positive R-axis (measured anti-clockwise) at this maximum expansion is denoted as θ_m. The mho circle's dynamic expansion is primarily influenced by b_m as shown in Fig. 1. This dynamic characteristic has been observed to enhance the mho element's resistive coverage. The steady-state operating point of the system before a fault occurrence is designated as "prefault" in Fig. 1 and Fig. 2.

A. SG-only system

During close-in faults, SGs exhibit voltage source behavior. Owing to the inertia of the SG, the voltage phase angle remains relatively unchanged from its pre-fault value. In Fig. 1, the magnitude of Z_{pol} is low for an SG-only system due to low pre-fault voltage and high fault current. Consequently, Z_{app} observed by the relay exhibits a small magnitude closer to the positive R-axis for the close-in fault with a fault resistance. Z_{pol} calculated from fault current and pre-fault voltage will be lower than pre-fault impedance and should be aligned more closely to the positive R-axis. This, in turn, makes b_m small, which is a result for Z_{pol} and Z_{app}. This results in a dynamic mho expansion with a diameter close to the actual mho circle.

B. GFOL PV-integrated system

In a GFOL PV-integrated system, the power electronics within the system impose a limit on the fault current. Consequently, the converter control will result in a fault voltage characterized by a reduced magnitude and a phase angle deviating from its pre-fault condition. Here Z_{app} will still be low and close to the positive R-axis, and Z_{pol} will have a magnitude and angle closer to pre-fault impedance. Thus, as shown in Fig. 2, b_m is much longer, and its angle, θ_m, is higher than that for the SG-only system, which reduces its resistive reach during positive power flow direction [7], [13], [18]. However, the initial dynamic mho expansion will be much bigger than that for the SG-only system.

Henceforth, within this work, a higher value of θ_m signifies that the memory vector b_m is moving away from the positive R -axis or negative X -axis and vice versa. The angle θ_m is measured from the positive R-axis in the anti-clockwise direction as shown in Fig. 1 and Fig. 2.

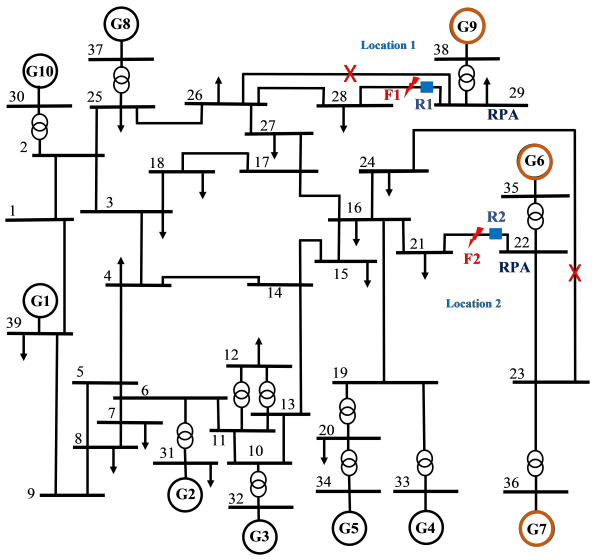

Fig. 3. Modified IEEE-39 bus system

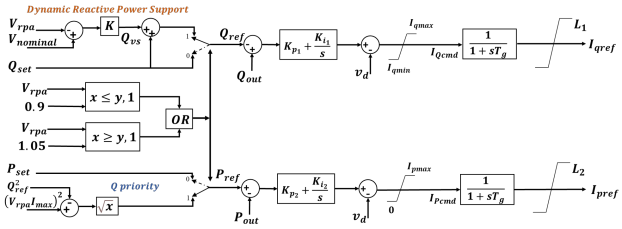

Fig. 4. Control logic for the GFOL PV generator

III. Test System Details

The IEEE 39-bus system, operating at 345 kV and 60 Hz, is adapted and simulated in PSCAD to ensure that the relays experience fault currents entirely supplied by PV generators, as depicted in Fig. 3. The Q-priority control strategy for the GFOL PV generator is illustrated in Fig. 4 [18]. This research utilizes phasor domain analysis, focusing on the 60 Hz fundamental frequency phasor observed by the relay while neglecting high-frequency switching dynamics, as harmonic behavior near switching frequencies is not within the study's scope. Consequently, the PV system is represented using an averaged model, and its control employs a Synchronous Reference Frame PLL with a Low Pass Filter (LSRF PLL) [18], [21]. The PV inverter is equipped with Low Voltage Ride-Through (LVRT) and High Voltage Ride-Through (HVRT) capabilities, implemented via dynamic voltage support, as shown in Fig. 5 [16]. For this analysis, solar irradiance and temperature are assumed to be constant.

At the Reference Point of Applicability (RPA), the voltage remains between 0.9 p.u. and 1.05 p.u. during steady-state operation [16]. Under these conditions, the Maximum Power Point Tracker (MPPT) output, P_{set}, is treated as P_{ref}, while Q_{ref} is initialized as $0.3287P_{set}$. The Proportional-Integral (PI) controller parameters for the PV control are fixed at K_{p1}=K_{p2}=0.05 and K_{i1}=K_{i2}=1 and T_g=0.02 s. When the voltage support feature is enabled, reactive power is provided

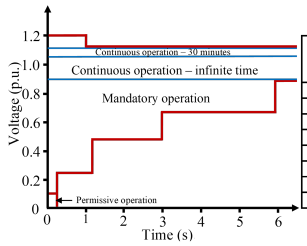

Voltage at RPA (p.u.)	Operating mode/response	Minimum ride-through time (s)
V>1.2	May ride-through / trip	NA
V>1.1	Mandatory operation	1
V>1.05	Continuous operation	1800
V<0.9	Mandatory operation	6
V<0.7	Mandatory operation	3
V<0.5	Mandatory operation	1.2
V<0.25	Mandatory operation	0.32
V<0.1	Permissive operation	0.32

Fig. 5. Low Voltage/High Voltage Ride-Through characteristics

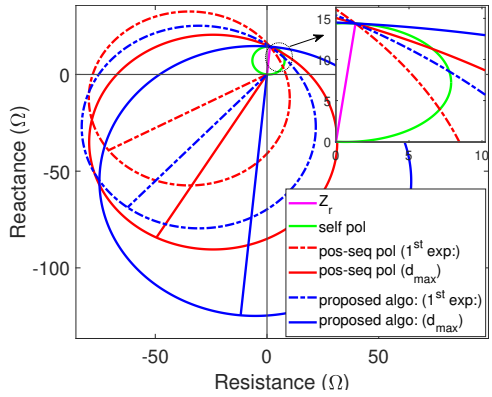

Fig. 6. First dynamic mho expansion (1^{st} exp:) and maximum dynamic mho expansion (d_{max}) for three-phase-to-ground fault seen by relay $R1$ when ω_m=0.5 for R_f=0 Ω

to support grid stability according to the grid codes. If the voltage deviates from acceptable limits, equations (4)-(6) are applied to determine the updated real and reactive power references. The voltage support mechanism generates additional reactive power, Q_{vs}, proportional to the deviation of the RPA voltage (V_{pv}) from the nominal voltage ($V_{nominal}$) using a K-factor [16], [18].

$$Q_{vs} = K(V_{nominal} - V_{pv}) \tag{4}$$

The K-factor can vary between 1 and 10 [17]. When the voltage support feature is enabled in Q-priority mode,

$$Q_{ref} = Q_{vs} + Q_{set} \tag{5}$$

$$P_{ref} = \sqrt{(V_{pv}I_{max})^2 - Q_{ref}^2} \tag{6}$$

Here, I_{max} is limited to 1.2 p.u. to constrain the inverter's output current [22]. All variables in the equations above are expressed in per-unit values.

IV. Proposed Algorithm Formulation

The positive sequence parameters in the memory voltage equation (1) are replaced with the phase voltage values as

$$V_{f,m}(i) = \omega_m V_{rf}(i) + (1-\omega_m)V_{f,m}(i-j) \tag{7}$$

where, V_{rf} is the fault voltage and $V_{f,m}$ is the memory voltage. All the voltages in (7) are phase values. Using phase memory voltage,Z_{pol} in (2) becomes

$$Z_{pol}(i) = \frac{V_{f,m}(i)}{I_{rf}(i)} \tag{8}$$

Dividing(7) by I_{rf}(i) we get,

$$\frac{V_{f,m}(i)}{I_{rf}(i)} = \omega_m \frac{V_{rf}(i)}{I_{rf}(i)} + (1-\omega_m)\frac{V_{f,m}(i-j)}{I_{rf}(i)} \tag{9}$$

Using Z_{app} from (2) and Z_{pol} from (8) in (9), we get

$$Z_{pol}(i) = \omega_m Z_{app}(i) + (1-\omega_m)\frac{V_{f,m}(i-j)}{I_{rf}(i)} \tag{10}$$

Now, using (3)

$$Z_{pol}(i) = \omega_m \{Z_{pol}(i) + b_m(i)\} + (1-\omega_m)\frac{V_{f,m}(i-j)}{I_{rf}(i)} \tag{11}$$

$$Z_{pol}(i) = \omega_m Z_{pol}(i) + \omega_m b_m(i) + (1-\omega_m)\frac{V_{f,m}(i-j)}{I_{rf}(i)} \tag{12}$$

$$\omega_m b_m(i) = Z_{pol}(i) - \omega_m Z_{pol}(i) - (1-\omega_m)\frac{V_{f,m}(i-j)}{I_{rf}(i)} \tag{13}$$

Now, substituting Z_{pol} from (8) and rearranging, we get

$$\omega_m b_m(i) = (1-\omega_m)\frac{V_{f,m}(i)}{I_{rf}(i)} - (1-\omega_m)\frac{V_{f,m}(i-j)}{I_{rf}(i)} \tag{14}$$

$$b_m(i) = \frac{(1-\omega_m)}{\omega_m}\left\{\frac{V_{f,m}(i)}{I_{rf}(i)} - \frac{V_{f,m}(i-j)}{I_{rf}(i)}\right\} \tag{15}$$

$$b_m(i) = \frac{(1-\omega_m)}{\omega_m}\{A\angle\theta_a\} \tag{16}$$

where

$$A\angle\theta_a = \frac{V_{f,m}(i)}{I_{rf}(i)} - \frac{V_{f,m}(i-j)}{I_{rf}(i)} \tag{17}$$

$$b_m(i) = b_m\angle\theta_m \tag{18}$$

(16) can be written as

$$b_m\angle\theta_m = \frac{(1-\omega_m)}{\omega_m})\{A\angle\theta_a\} \tag{19}$$

In (19), ω_m is considered as a scalar value between 0 and 1. As a result, the angle of the memory vector b_m, θ_m, will be the angle of the vector A, θ_a. However, if ω_m is considered as a complex value, $\omega_m\angle\theta_\omega$, the angle of the vector b_m, θ_m, will depend on both θ_a and θ_ω. The equation (19) can be modified with complex weight factor as,

$$b_m\angle\theta_m(i) = \frac{(1-\omega_m\angle\theta_\omega)}{\omega_m\angle\theta_\omega}\{A\angle\theta_a\} \tag{20}$$

Hence, the angles of the vectors in (18) can be written as,

$$\theta_m = \angle(\frac{(1-\omega_m\angle\theta_\omega)}{\omega_m\angle\theta_\omega}) + \theta_a \tag{21}$$

$$\theta_m = \angle\left\{(\frac{1}{\omega_m}\angle-\theta_\omega) - 1\right\} + \theta_a \tag{22}$$

When θ_ω is zero, when ω_m is a scalar, from (22)

$$\theta_a = \theta_m \tag{23}$$

Hence, the initial value of θ_a can be obtained from the angle, θ_m, of the first memory vector keeping ω_m as a scalar value. After obtaining the θ_a, it can be substituted in (22).

The problem with the maximum expansion of PSMP mho relay in the presence of IBR is the reduction in resistive

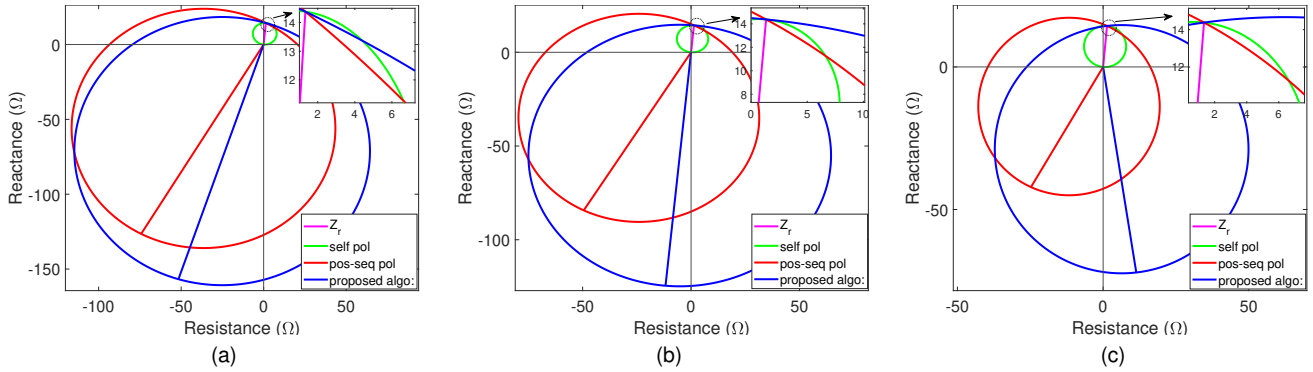

Fig. 7. Maximum dynamic mho expansion for three-phase-to-ground fault seen by relay $R1$ for R_f=0 when (a) ω_m=0.25 (b) ω_m=0.5 (c) ω_m=0.75

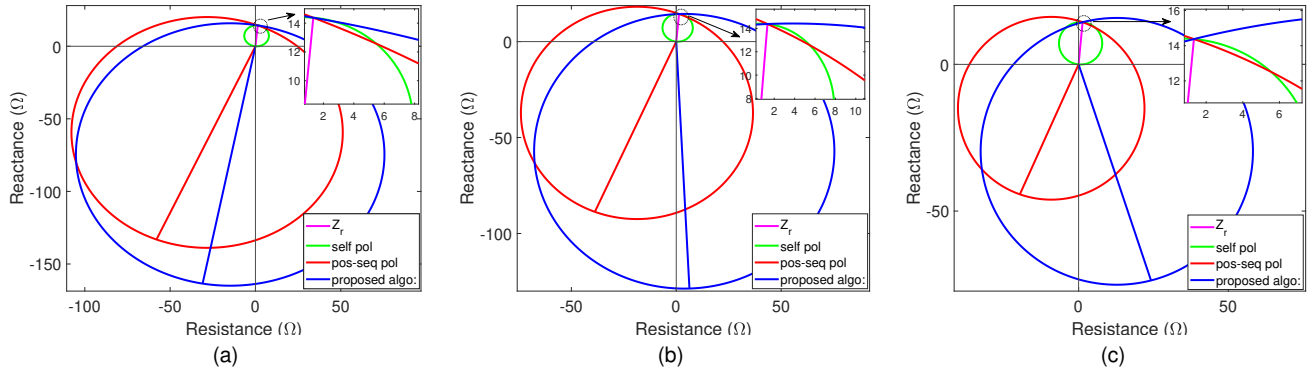

Fig. 8. Maximum dynamic mho expansion for three-phase-to-ground fault seen by relay $R1$ for R_f=5Ω when (a) ω_m=0.25 (b) ω_m=0.5 (c) ω_m=0.75

reach due to the increased $b_m\angle\theta_m$. One of the solutions is to bring the memory vector b_m along the line of Z_r such that $|\theta|+|\theta_m|$=180°. Both angles are measured from the positive R axis and are of opposite sign. θ is positive while θ_m is negative. Hence, for the memory vector to be along Z_r,

$$\theta_m = \theta - 180^\circ \tag{24}$$

On using (23) and (24) in (22), we get

$$\theta - 180^\circ - \theta_a = \angle\left\{(\frac{1}{\omega_m}\angle - \theta_\omega) - 1\right\} \tag{25}$$

Expanding the right hand side of (25), we get

$$\theta - 180^\circ - \theta_a = \angle\left\{\frac{1}{\omega_m}cos(-\theta_\omega) + j\frac{1}{\omega_m}sin(-\theta_\omega) - 1\right\} \tag{26}$$

$$\theta - 180^\circ - \theta_a = tan^{-1}\frac{\frac{1}{\omega_m}sin(-\theta_\omega)}{\frac{1}{\omega_m}cos(-\theta_\omega) - 1} \tag{27}$$

$$tan(\theta - 180^\circ - \theta_a) = \frac{\frac{1}{\omega_m}sin(-\theta_\omega)}{\frac{1}{\omega_m}cos(-\theta_\omega) - 1} \tag{28}$$

where, θ is the phase angle of Z_r, the impedance reach of the protected line, and θ_a is obtained from (23). Both the angles are known to solve the (28) to get θ_ω. Once θ_ω is obtained, we use this value to calculate the complex weight factor $\omega_m\angle\theta_\omega$ for the remaining protection passes. The magnitude of the weight factor, ω_m, is kept the same in all the protection passes.

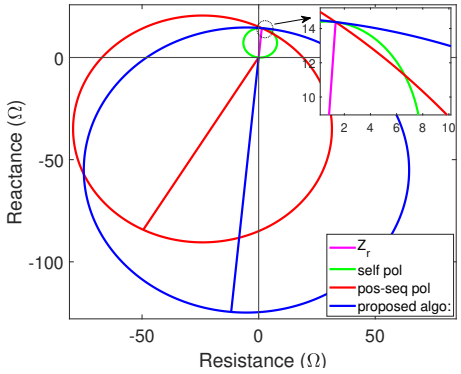

Fig. 9. Maximum dynamic mho expansion for single-line-to-ground fault seen by relay $R1$ when ω_m=0.5 for R_f=0

For the different types of faults considered, the polarizing quantities for positive-sequence memory polarization and the proposed phase memory polarization are shown in Table I. Subscripts 'A', 'B', and 'C' represent phases A, B, and C, respectively. The superscript '+' represents the positive-sequence component, and the subscript 'm' represents the memory component.

V. Analysis of Results

Post-processing calculations were performed on fault data extracted from simulations conducted at a sampling rate of 3.84 kHz, capturing 64 samples per cycle. The analysis considered eight protection zones within each cycle. To

TABLE I
POLARIZING QUANTITIES OF RELAY ELEMENTS

Fault Type	Relay element	Fault voltage (V_{rf})	Positive sequence memory pol:		Proposed algorithm	
			Polarizing voltage	Fault current (I_{rf})	Polarizing voltage	Fault current (I_{rf})
Three-phase-to-ground	AG	V_A	$V^+_{f,m}$	I_A	$V^A_{f,m}$	I_A
Single-line-to-ground	AG	V_A	$V^+_{f,m}$	$I_A + K_0 \cdot I_0$	$V^A_{f,m}$	$I_A + K_0 \cdot I_0$
Line-to-line	AB	$V_A - V_B$	$-j \cdot a \cdot V^+_{f,m} \cdot \sqrt{3}$	$I_A - I_B$	$-j \cdot a \cdot V^A_{f,m} \cdot \sqrt{3}$	$I_A - I_B$

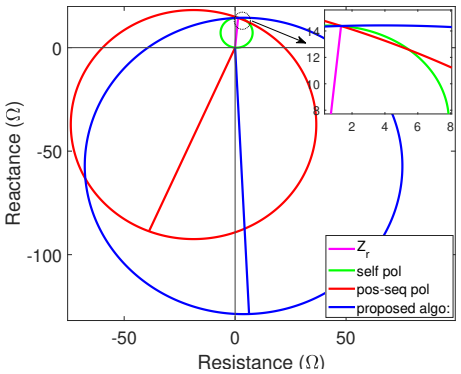

Fig. 10. Maximum dynamic mho expansion for single-line-to-ground fault seen by relay $R1$ when ω_m=0.5 for R_f=5 Ω

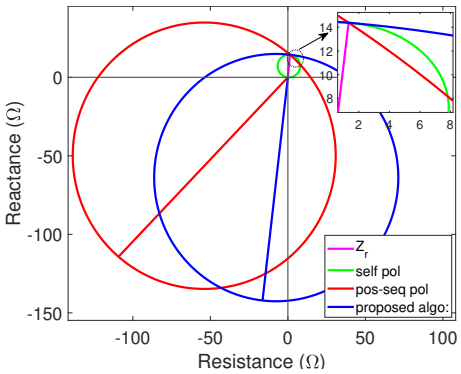

Fig. 11. Maximum dynamic mho expansion for line-to-line fault seen by relay $R1$ when ω_m=0.5 for R_f=0

determine the memory voltage for the preceding two cycles, j is set to 16 in the memory voltage calculation equations, (1) and (7). The study investigated the maximum attainable expansion of the dynamic mho characteristic of the PSMP mho element in a PV-integrated system. This was achieved by comparing the maximum dynamic mho expansion for the positive-sequence memory polarization and the proposed phase memory polarization algorithms while also examining self-polarized mho characteristics.

For this analysis, the existing generator $G9$ of the IEEE 39 bus system connected to Bus 38 was substituted with an 870.5 MVA, 33 kV GFOL PV generator. Subsequently, line $26-29$ was removed from the system model. A load flow analysis was then conducted on this modified system configuration. This specific arrangement isolates the fault current experienced by relay $R1$, ensuring its sole contribution originates from the PV generator (refer to Fig. 3). The pre-fault power flow direction seen by relay $R1$ is positive. A fault, designated as $F1$, was

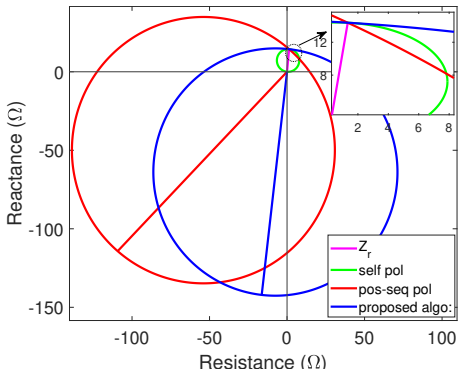

Fig. 12. Maximum dynamic mho expansion for line-to-line fault seen by relay $R1$ when ω_m=0.5 for R_f=5 Ω

simulated on lines $28-29$ at a distance of 2% from relay $R1$ for a duration of 0.07 s.

1) Three-phase-to-ground fault: Three-phase-to-ground faults have been analyzed in this section. Here, fault $F1$ is a three-phase-to-ground fault. The reduction in resistive reach during the first dynamic mho expansion after fault initiation and subsequent maximum dynamic mho expansion for positive sequence memory polarization and the proposed phase memory polarization are shown in Fig. 6. While the maximum mho expansion exhibits a reduced resistive reach compared to the initial mho expansion, it is crucial to acknowledge potential negative ramifications. Notably, the proposed algorithm demonstrates a clear enhancement in the resistive reach of the mho circle, even from the first dynamic mho expansion. Henceforth, only the maximum dynamic mho expansion in terms of maximum diameter, d_{max}, and memory vector angle, θ_m have been compared for the positive sequence memory polarization and the proposed phase memory polarization techniques. Results have been presented for a varying weight factor (ω_m), fault resistance (R_f), and fault location. The maximum mho expansion seen by relay $R1$ for weight factors of ω_m=0.25, 0.5 and 0.75 and zero fault resistance are shown in Fig. 7a, Fig. 7b and Fig. 7c, respectively. Analysis reveals that maximum mho expansion utilizing positive sequence memory polarization (red curve) results in a curtailed resistive reach for the GFOL PV-integrated system. Conversely, the proposed algorithm (blue curve) demonstrates the capability to effectively restore the resistive reach. The observed outcomes remain consistent across the range of weight factors investigated. The proposed algorithm has also been verified for a fault resistance of 5 Ω. The results are shown in Fig. 8a, Fig. 8b and Fig. 8c.

TABLE II
COMPARISON OF POSITIVE-SEQUENCE MEMORY POLARIZATION AND PROPOSED ALGORITHM FOR A GFOL PV INTEGRATED SYSTEM FOR VARYING FAULT TYPES AND ω_m=0.5, R_f=0

Fault Type	Positive sequence memory pol:			Proposed algorithm		
	ω_m	d_{max}	θ_m	$\omega_m \angle \theta_\omega$	d_{max}	θ_m
Three-phase-to-ground	0.5	111.01	-120.412	$0.1749 - 0.1787j$	179.15	-108.23
Single-line-to-ground	0.5	175.83	-131.95	$0.4267 - 0.2606j$	135.001	-94.37
Line-to-line	0.5	169.63	-133.72	$0.3985 - 0.3020j$	157.49	-96.56

2) Single-line-to-ground fault: Here, fault $F1$ is a single-line-to-ground fault at phase A. The comparison of maximum dynamic mho expansion for positive sequence memory polarization and proposed method considering ω_m=0.5 is shown in Fig. 9 and Fig. 10 for R_f=0 and R_f=5Ω, respectively. It has been observed that the proposed method improves the resistive reach as in the previous cases. The results have been verified for ω_m= 0.25 and 0.75 for both the fault resistances.

3) Line-to-line fault: Here, fault $F1$ is a line-to-line fault between phases A and B. A comparative analysis of the maximum dynamic mho expansion for both the positive sequence memory polarization and the proposed method for ω_m=0.5 are shown in Fig. 11 and Fig. 12 for R_f=0 and R_f=5Ω, respectively. Consistent with previous observations, the proposed method demonstrates an improved resistive reach. These findings were further validated for ω_m= 0.25 and 0.75 across both the fault resistances.

A comparison of the positive-sequence memory polarization and the proposed algorithm for a GFOL PV integrated system for varying fault types with ω_m=0.5 and R_f=0 is presented in Table II. The results have also been verified for a second location, L2, shown in Fig. 1.

VI. CONCLUSIONS

This paper comprehensively investigates the dynamic performance of memory-polarized mho relays in power systems with significant GFOL PV generation. This paper delves into the dynamic behavior of these relays, analyzing the impact of IBR transients on the maximum expansion of dynamic mho (d_{max}) and memory vector angle (θ_m) of the expanded mho characteristic. Through rigorous simulations of various fault scenarios, including three-phase-to-ground, single-line-to-ground, and line-to-line faults, the study identifies a possibility of decline in the resistive reach of positive-sequence memory-polarized mho relays in the presence of GFOL PV generation. To address these challenges, a novel algorithm incorporating a complex weight factor is proposed. This approach shifts the memory vector more towards the positive R-axis and hence helps to recover the resistive reach. The proposed method is power priority agnostic. The effectiveness of the proposed algorithm is rigorously evaluated across a range of fault types, weight factor values, fault resistances, and locations, demonstrating its potential to improve overall system security.

REFERENCES

[1] Y. Guo, B. C. Pal, R. A. Jabr and H. Geng, "Global Optimality of Inverter Dynamic Voltage Support," *IEEE Trans. Power Syst.*, vol. 37, no. 5, pp. 3947-3957, Sept. 2022.

[2] C. Canizares et al., "Benchmark systems for small signal stability analysis and control," IEEE PES-TR18, Tech. Rep., 2015.

[3] S. Paladhi and A. K. Pradhan, "Adaptive Distance Protection for Lines Connecting Converter-Interfaced Renewable Plants," *IEEE J. Emerg. Selec. Topics Power Electron.*, vol. 9, no. 6, pp. 7088–7098, Dec. 2021.

[4] J. J. Chavez, M. Popov, D. López, S.Azizi, and V. Terzija, "S-Transform based Fault Detection Algorithm for Enhancing Distance Protection Performance," *Int. J. Electr. Power Energy Syst.*, Vol. 130, 2021.

[5] M. J. B. B. Davi, M. Oleskovicz, F. V. Lopes, et al., "A Case Study-Based Review of the Impacts of Inverter-Interfaced Wind Power Plants on Distance Protections," *J. Control. Autom. Electr. Syst. 34*, 2023.

[6] B. Kasztenny, "Distance Elements for Line Protection Applications Near Unconventional Sources.", SEL Inc., Nov. 2022

[7] D. D. Fentie, "Understanding the Dynamic Mho Distance Characteristic," in 2016 69th Annual Conference for Protective Relay Engineers (CPRE), IEEE, 2016, pp. 1–15.

[8] S. Cao, Q. Hong, D. Liu, L. Ji and C. Booth, "Impact of converter equivalent impedance on distance protection with the MHO characteristic," 17th International Conference on Developments in Power System Protection (DPSP 2024), Manchester, UK, 2024, pp. 336-342.

[9] Y. Liang, W. Li and W. Zha, "Adaptive Mho Characteristic-Based Distance Protection for Lines Emanating From Photovoltaic Power Plants Under Unbalanced Faults," *IEEE Syst. J.*, vol. 15, no. 3, pp. 3506-3516, Sept. 2021.

[10] B. Kasztenny and M. V. Mynam, "Distance Element Polarizing Logic for Systems with Low Inertia," 17th International Conference on Developments in Power System Protection (DPSP 2024), Manchester, UK, 2024, pp. 122-131.

[11] V. Chakrapani, I. Voloh, P. Horton and S. Swain, "Assessing the Performance of an Enhanced Distance Relay in Converter-Dominated Network," 17th International Conference on Developments in Power System Protection (DPSP 2024), Manchester, UK, 2024, pp. 162-167.

[12] A. Haddadi, M. Zhao, I. Kocar, E. Farantatos, and F. Martinez, "Impact of Inverter-Based Resources on Memory-Polarized Distance and Directional Protective Relay Elements," 2021 52nd North American Power Symposium (NAPS), Tempe, AZ, USA, 2021.

[13] A. Radhakrishnan, A. Ghosh, I. R. Sai Priyamvada and S. Das, "Performance of Memory-Polarized Distance Relay in Presence of PV Generator with VdC-Q Control," IEEE Energy Conversion Congress and Exposition (ECCE), Detroit, MI, USA, 2022, pp. 1-8.

[14] A. Radhakrishnan, I. R. S. Priyamvada and S. Das, "Impact of P – Q Control based PV Generator on Memory-Polarized Mho Relay," 2022 International Conference on Smart Energy Systems and Technologies (SEST), Eindhoven, Netherlands, 2022, pp. 1-6.

[15] E. Sorrentino, J. Melián, and V. De Andrade, "A Novel Method to Obtain the Offset Mho Characteristic of Memory-Polarized and Cross-Polarized Distance Functions of Protective Relays from Experimental Measurements," *Electric Power Syst. Res.*, Vol. 216, 2023.

[16] "IEEE Standard for Interconnection and Interoperability of Inverter-Based Resources (IBRs) Interconnecting with Associated Transmission Electric Power Systems," in IEEE Std 2800-2022, vol., no., pp.1-180, 22 April 2022.

[17] M. J. B. B. Davi, M. Oleskovicz, F. V. Lopes, " Study on IEEE 2800-2022 Standard Benefits for Transmission Line Protection in the Presence of Inverter-Based Resources," *Electric Power Syst. Res.*, Vol. 220, 2023.

[18] M. Jayamohan, S. Das and M. Popov, "Sensitivity of Dynamic Mho Characteristic to PLL Parameters of Grid Following PV," 2024 IEEE International Communications Energy Conference (INTELEC), Bengaluru, India, 2024, pp. 1-6
[19] E. O. Schweitzer, “New developments in distance relay polarization and fault-type selection", Proc. 16th Annu. Western Protective Relay Conf., pp. 1-19, Oct. 1991.
[20] D. Hou, A. Guzman, and J. Roberts, “Innovative solutions improve transmission line protection," Proc. Southern African Conf. Power Syst. Protect., pp. 1-25, Nov. 1998.
[21] R. T. Elliott, A. Ellis, P. Pourbeik, J. J. Sanchez-Gasca, J. Senthil and J. Weber, “Generic Photovoltaic System Models for WECC - A Status Report,” 2015 IEEE PES General Meeting (PESGM), Denver, CO, USA, Jul. 2015, pp. 1–5.
[22] “Modification of Commercial Fault Calculation Programs for Wind Turbine Generators,” IEEE PESTR-78, Tech. Rep., June 2020.